Research on a new high-quality and high-efficiency SLM forming method based on interlayer strategy

Peng Wang[1, 2], Dongju Chen[1, 2] and Gang Li [1, 2]

[1] Mechanical Industry Key Laboratory of Heavy Machine Tool Digital Design and Testing, Faculty of Materials and Manufacturing, Beijing University of Technology, Beijing 100124, China.
[2] Beijing Key Laboratory of Advanced Manufacturing Technology, Faculty of Materials and Manufacturing, Beijing University of Technology, Beijing 100124, China.

Abstract. To ensure the forming quality of SLM and to improve the forming efficiency of SLM, this paper investigates the forming effect of Ti6Al4V specimens formed by SLM based on an interlayer strategy. The conditions for improving the relative density of the specimens are high laser power, small point distance, long exposure time and long hatch spacing. High laser power provides sufficient laser energy density in the formation of thicker powder layers, reduced point distance ensures wetting behavior of the melt pool, longer exposure time provides the time required to fully melt the powder and increased hatch distance facilitates dispersion of the laser energy density. Process parameters have a strong influence on the relative density of SLM formed specimens, and by adjusting the process the highest density of 99.99% can be achieved. The microstructure of the specimens consisted mainly of acicular martensite α' and columnar β grains due to the effects of repeated thermal cycling. Due to the presence of martensite α', the tensile and yield strengths of the specimens are increased, but the elongation of the specimens is reduced.

Keywords: Selective laser melting; keywords covered; microstructure and mechanical properties.

1. Introduction

Ti6Al4V is the most common nonferrous alloy and is widely used in aerospace, marine, and biomedical applications [1]. It has long-term biocompatibility, excellent strength-to-weight ratio, superior corrosion resistance, outstanding low-temperature brittleness resistance, and high fracture toughness. Despite its many advantages, Ti6Al4V has proven to be a difficult material to machine. There is significant material waste, long lead times, and high manufacturing costs using conventional casting, forging, and rolling processes [2]. Selective laser melting (SLM) technology uses a laser beam and metal powder as the fabrication tool, eliminating the need for traditional fabrication tools such as fixtures or molds, thereby significantly reducing the processing cycle time [3].

Improving the efficiency of SLM has been a hot research direction in the field of additive manufacturing. Currently, the forming efficiency can be improved by using multiple lasers, but the more important purpose of using multiple lasers is to increase the size of SLM formed parts. In previous research, smaller layer thicknesses are generally used to ensure forming accuracy and quality, which leads to a decrease in forming efficiency. Compared with increasing the scanning speed, using a high layer thickness can reduce the melting time per-layer and thus have a higher forming efficiency. Increasing the layer thickness by about 1.6 times can reduce the fabrication time by 40% while maintaining reasonable surface roughness [4]. Savalani et al. [5] investigated the effect of layer thickness on magnesium formed by SLM and found that the specimens with low layer thickness had smoother and flatter surfaces. When the thickness increased, the surface exhibited higher surface roughness values. Sufiiarov et al. [6] investigated the relationship between the layer thickness and the relative density, microstructure and mechanical properties of nickel-based superalloys formed by SLM. It was found that specimens with a layer thickness of 30μm had higher strength and lower elongation than those with a layer thickness of 50μm. Nguyen et al [7] prepared Inconel 718 specimens with different powder layer thicknesses (20, 30, 40 and 50μm). The results showed that the thinner the layer thickness, the higher the relative density and the higher the dimensional accuracy. The study by Greco [8] showed that thicker powder layers would lead to a decrease of relative density and a decrease of microhardness due to the limited depth of laser energy penetration into the powder layer. The results of GAO et al. [9] showed that the relative density increases gradually with decreasing laser volume energy density when the layer thickness is less than or equal to 40μm, while the relative density increases and then decreases with decreasing laser volume

energy density when the layer thickness is greater than 40μm.

Previous studies have shown that increasing the layer thickness can improve the forming efficiency, but to a certain extent it will affect the quality of the formed specimen. Therefore, using the appropriate layer thickness at the appropriate part of the specimen is the key to ensure the high-quality and high-efficiency forming of the formed specimen. This paper focuses on a new process approach to improve forming efficiency using interlayer strategies to ensure higher forming efficiency in parts that require efficient forming. The effects of process parameters on the wettability, relative density, defects, microstructure and mechanical properties of specimens formed by the interlayer strategy are investigated in detail by single track and multi-layer SLM fabrication.

2. Experimental details

2.1 Materials and experimental equipment

The experiment uses the gas atomized Ti6Al4V powder material produced by Falcontech. The powder is nearly spherical particles (shown in Fig. 1a), with a particle size range of 15-53μm (Fig. 1b). The particle size detected by the laser particle size analyzer is D10: 16.4μm, D50: 32.13μm, D90: 57.54μm. The experiment was completed in the AM400 (Renishaw plc, London, UK) laser melting forming equipment. The entire experiment was carried out in a closed cabin filled with argon as a protective gas. AM400 uses a continuous laser mode with a maximum forming power of 400W and an Nd: YAG laser with a wavelength of 1075nm.

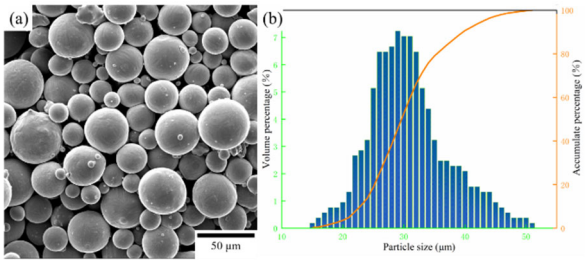

Fig. 1 Powder (a) morphology of Ti6Al4V; (b) particle size distribution of Ti6Al4V

The experiment aims to improve the forming efficiency and ensure the forming quality. The forming strategy of only spreading powder on some layers without laser forming is used to improve the forming efficiency. As shown in Fig. 2, the powder spreader does not perform laser forming after spreading a layer of powder and then spreading a layer of powder without laser forming. When spreading the third layer of powder, the laser forms the specimen according to preset parameters. In this way, the efficient strategy of the interlayer strategy is realized. Assuming that the preset layer thickness is 50μm and the actual layer thickness is 150μm, efficient forming is achieved, while the high quality forming strategy using preset layer thickness forming in critical areas can be realized. The preset experiment scanning strategy is based on the curved scanning strategy, i.e., the angle between the Nth and N+1th layers is 67°.

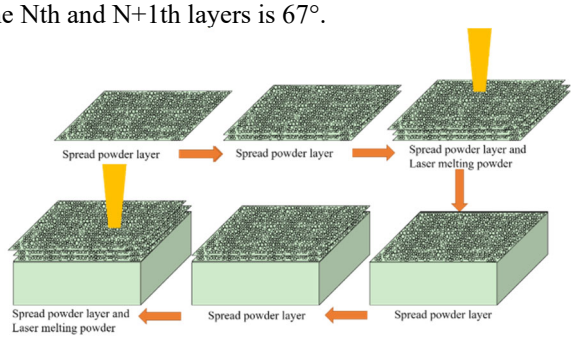

Fig. 2 Schematic diagram of the interval of the powder layer thickness

2.2 2.2 Experimental methods

The laser power, exposure time, and point distance of the single track formed on the specimen-substrate were respectively set to 300-350W (in an increment of 50W), 40-120μs (in an increment of 20μs), and 35-105μm (in an increment of 17.5μm). The preset layer thickness is 50μm, and the actual layer thickness is 150μm based on the interlayer strategy shown in Fig. 2. Table 1 shows the process parameters used in the single track. Based on the experimental results of the single track, circular fabricated parts with a diameter of 8mm were prepared according to the parameters shown in Table 2 to evaluate the quality of the process parameters. After slicing the multilayer blocks with wire cutting equipment (Cmne, Beijing, China), the metallographic specimens are grinded and polished according to standard metallographic procedures, and then processed with Kroll reagent (2ml HF, 6ml HNO3, and 90ml H2O solution) for etching. Images of specimen cross-sections were analyzed and measured using ImageJ (NIH, Bethesda, MD, USA) to calculate the relative density. The morphology of the single-track and multi-layer specimens was observed with an optical microscope (VK-X200, KEYENC, Japan), and the microstructure of the specimens was observed with a scanning electron microscope (SEM) (Phenom XL; Holland). A universal tensile testing machine (5966; Instron, Boston, MA, USA) was used to test the specimen at a tensile rate of 0.01 mm/s at room temperature.

Table 1 Process parameters of the single-track experiments

Parameter	Value	Increment
Laser Power (W)	300-350	50
Layer thickness (μm)	150 (actual layer thickness)	--
Exposure time (μs)	40-120	20
Point distance (μm)	35-105	17.5

Table 2 The process parameters of the different multilayer fabrication specimens

Parameter	Value	Increment
Laser Power (W)	380	--
Layer thickness (μm)	150 (actual layer thickness)	--
Exposure time (μs)	100-220	20-40
Point distance (μm)	25-65	10-15
Hatch spacing (μm)	50-110	20

3. Results and discussion

3.1 Single-track SLM experiments

Uniform, smooth and stable single-tracks are the guarantee for obtaining high relative density specimens. The morphology of the single-tracks under different process parameters is shown in Fig. 3. The horizontal coordinate indicates the point distance, with the values increasing from 35 to 105μm (in an increment of 17.5μm), and the vertical coordinate indicates the exposure time, with the values increasing from 40μs to 120μs (in an increment of 20μs). As shown in Fig. 3 (a-b), at the laser power of 300W, the single track shows an unstable or even distorted form when the exposure time is less than 100μs or the point distance is greater than 70μm. This is because the exposure time is too short or the point distance is too large, and the laser energy density of the laser input cannot completely melt the powder. When the exposure time is longer than 100μs or the point distance is less than 52.5μm, the laser energy density can reach a moderate state and the single-track is stable. As shown in Fig. 3 (c-d), a stable single track can be obtained when the laser power is 350W, at a point distance of 35μm and the exposure time higher than 60μs. When the point distance increases, it is not easy to ensure the wettability of the molten pool, and the single-track presents a distorted state. This is because the relatively high laser energy density at high laser power tends to lead to instability of the melt pool, but the high laser power can ensure sufficient melting of the thick powder layer. Compared with Fig. 3, the high laser power can ensure the stability of the single track in the relatively large floating range of exposure time.

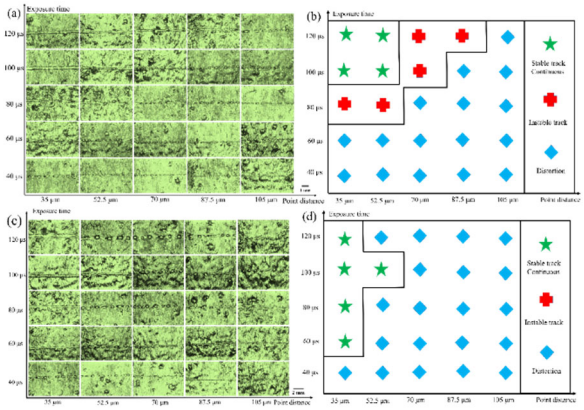

Fig. 3 Morphological characteristics of single-track (a) surface characteristics under the laser power of 300W; (b) process results of (a); (c) surface characteristics under the laser power of 350W; (d) process results of (c)

3.2 Multi-layer SLM fabrication

Based on experimental research of single-track, high laser power allows for a wide range of floating process parameters. In this section, the exposure time, point distance and hatch spacing were set to 100-220μs (in increments of 20-40μs), 25-65μm (in increments of 10-15μm) and 50-110μm (in increments of 20μm), respectively, in order to fully investigate the process required to achieve high relative density of the specimens.

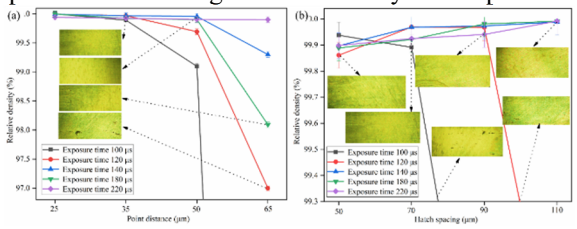

Fig. 4 Relative density curve (a) relative density curve under same hatch spacing; (b) relative density curve under different hatch spacing

As shown in Fig. 4(a), the optimal combination of exposure time and point distance was investigated at a hatch spacing of 70μm. At a fixed exposure time, the relative density showed a decreasing trend with the increase of the point distance. This is because the lap quality between the melt pools becomes poorer as the point distance increases, leading to more un-melted defects between the melt pools. Sufficient laser energy density can be ensured to melt the powder with a small point distance. In addition, a higher relative density can be maintained at the higher exposure time. This is because the actual layer thickness of the interlayer strategy is 150μm, while thicker powder layers require longer melting time to ensure complete melting of the powder. As shown in Fig. 4(b), the fixed point distance is 35μm, and the optimal combination of exposure time and hatch spacing is investigated. As the hatch spacing increases, the relative density shows an increasing trend at a fixed exposure time. This is because the energy density is higher at high laser power and small point distance, and increasing the hatch spacing can help disperse the laser energy density. When the exposure time is 100-120μs, the

relative density is unstable. As the hatch spacing increases, un-melted defects appear between the melt pools. The longer exposure time allows a larger floating space for the hatch spacing. In this experiment, the relative densities of most of the formed specimens were higher than 99%, and the highest density could reach 99.99%.

The main reason affecting the relative density is defects due to the choice of process parameters. When the powder melts into a liquid and then solidifies rapidly, defects such as holes and inclusions will inevitably appear due to shrinkage of the melt, transient stresses, and the presence of gases and impurities [10]. In this section, the mechanism of defect formation is investigated by analyzing the cross-section of the specimen.

Fig. 5 shows the defects that resulted in the decrease of relative density. Fig. 5(a) shows the un-melted defects between the molten pools and un-melted powder can be observed in the un-melted region. Fig. 5(b) shows the microporous defects in the molten pool, and Fig. 5(c) shows the spheroidization inside the specimen. The defect of un-melted defects between the molten pools is caused by poor adhesion of the molten pool, as shown in Fig. 5(d). This defect is mainly caused by the improper selection of process parameters (too large setting of point distance or hatch spacing is the main cause of un-melted defects between molten pools). One is that the gas cannot escape from the bottom of the molten pool during solidification and cooling because the solubility of the gas decreases and the gas cannot be released in time, as shown in Fig. 5(e). Another reason for the micropores is that the gas in the hollow powder did not escape in time, as shown in Fig. 5(f). Spheroidization defects are mainly caused by splashing during the forming process. The spattered particles solidify during the flying process and partly fall into the molten pool and form spheroidization inside the specimen after solidification. Some of the splashes splashed onto the surface of the solidified specimen, forming surface spheroidization. Some spatters fall on the unformed powder and form inclusions. After being melted, internal spherification of the specimen may also form, as shown in Fig. 5 (g). The cause of the defect may also be the poor wetting between the single-track and the substrate, as shown in Fig. 5 (h-i). When the single-track and the substrate do not bond well, internal porosity or spherification can result.

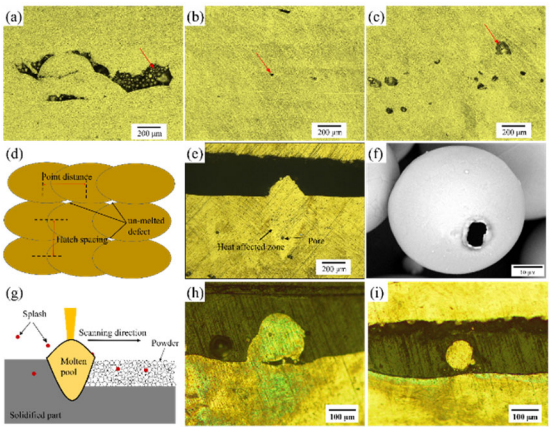

Fig. 5 Internal defects of formed specimens (a) un-melted defects between the molten pools; (b) pore defects; (c) slag inclusion defects; (d) schematic diagram of the formation of un-melted defects between the molten pools; (e) keyhole defect; (f) hollow powder; (g) schematic diagram of the formation of spheroidization defects; (h) single-track with poor wettability; (i) spheroidization

3.3 Microstructure and mechanical properties

The microstructure of the specimen based on the interlayer strategy as shown in Fig. 6. During the solidification of the specimen, mainly acicular martensite α' and columnar β grains are generated, and martensite α' fills and occupies the columnar β grains. As shown in Fig. 6(a), martensite α' can be continuously derived by iteration, and the derivatives are perpendicular to the nascent martensite α'. The martensite α' on both sides of the columnar β grain boundary shows different morphologies, as shown in Fig. 6(b). By observation, it can be found that the top martensite α' of the formed specimen is relatively coarse (Fig. 6c) and the bottom martensite α' is relatively fine. This is because, with the continuous stacking of formed layers, the heat input from the newly formed layers affects the already formed areas (as shown in Fig. 5e). The bottom part has many repetitive thermal cycles, and the fine martensitic α' structure is easily formed by successive iterations. On the other hand, the top has less repetitive thermal cycles and the coarse martensitic α' structure of the first iteration is easily formed.

The tensile strength and yield strength of the specimens formed by SLM based on the interlayer strategy are higher than that of the forged and cast specimens, but the elongation is lower than that of the forged and cast specimens. The existence of martensite α' guarantees the strength of the specimen but reduces the plasticity of the specimens. Numerous studies have shown that the SLM-formed Ti6Al4V specimens suffer from low elongation [11-13], but the elongation of SLM-formed specimens can still be improved by post-treatment methods such as heat treatment or adding reinforcement [14-16]. Fig. 7 shows the fracture topography of the tensile specimen. There are usually pores and other defects at the fracture, which reduces the strength of the specimen at this location, as shown in Fig. 7 (c-d). The fracture modes of tensile specimens include ductile fracture and brittle fracture. As shown in Fig. 7(a), the region without ductile deformation

is mainly composed of the cladding formed after the solidification of the molten pool. The ductile deformation region consists of small and shallow dimples, and these dense dimples increase the strength of the formed specimen, as shown in Fig. 7(b).

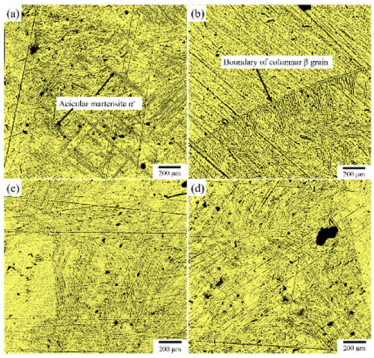

Fig. 6 Microstructure

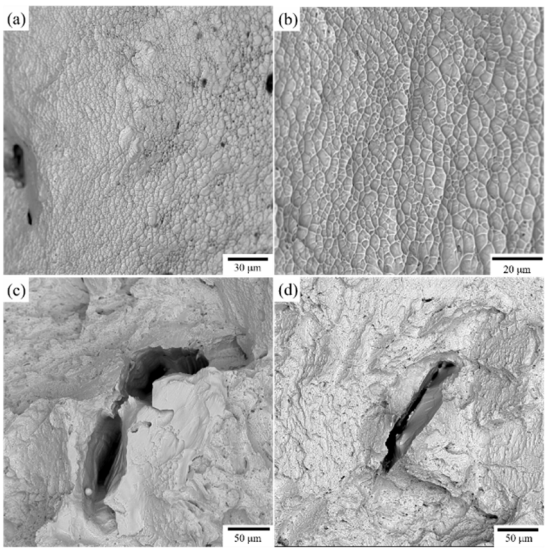

Fig.7 Morphology of tensile fracture surface (a) plastic deformation; (b) pore defects; (c-d) fracture caused by porosity

4. Summary

In this paper, the forming quality of Ti6Al4V specimens formed by SLM based on interlayer strategy was investigated. The effects of process parameters on the wettability, relative density, defects, microstructure and mechanical properties of the specimens were analyzed by single-track and multilayer fabrication. The following conclusions were drawn:

1. The single-track experiment shows that it is not easy to ensure the wettability of the molten pool by increasing the point distance in the thicker layers forming environment. High laser power can ensure adequate melting of thick powder layers, and high laser power can ensure that the single track is stable over a relatively large floating range of exposure times.

2. Multilayer fabrication experiments show that small point distance ensures sufficient laser energy density to melt the powder, while longer exposure times maintain high relative densities. Increasing the hatch spacing can help to disperse the laser energy density and increase the relative density of the specimens at high laser power and small point distance. In this experiment, the relative density of most of the formed specimens is higher than 99%, and the highest density can reach 99.99%.

3. During solidification of the specimens, mainly acicular martensite α' and columnar β grains are generated, and martensite α' can be continuously derived by iteration. Due to the effect of repeated thermal cycling, the bottom martensite α' of the formed specimens is relatively small and the top martensite α' is relatively coarse. Due to the effect of microstructure, the experimental tensile and yield strengths are higher than those of the forged and cast specimens, but the elongation is lower than that of the forged and cast specimens.

References

1. de Souza A F, Al-Rubaie K S, Marques S, et al. Effect of laser speed, layer thickness, and part position on the mechanical properties of maraging 300 parts manufactured by selective laser melting. Materials Science and Engineering: A. Vol. 767 (2019) p. 138425.
2. Zhu Y, Zou J, Yang H. Wear performance of metal parts fabricated by selective laser melting: a literature review. Journal of Zhejiang University-SCIENCE A. Vol. 19 (2018) No. 2, p. 95-110.
3. Todd I. No more tears for metal 3D printing. Nature. Vol. 549 (2017) No. 7672, p. 342-343
4. Martin J H, Yahata B D, Hundley J M, et al. 3D printing of high-strength aluminium alloys. Nature. Vol. 549 (2017) No. 7672, p. 365-369.
5. Savalani M M, Pizarro J M. Effect of preheat and layer thickness on selective laser melting (SLM) of magnesium. Rapid Prototyping Journal. Vol. 22 (2016) No. 1, p. 115-122.
6. Sufiiarov V S, Popovich A A, Borisov E V, et al. The effect of layer thickness at selective laser melting. Procedia engineering. Vol. 174 (2017) No. 7672, p. 126-134.
7. Nguyen Q B, Luu D N, Nai S M L, et al. The role of powder layer thickness on the quality of SLM printed parts. Archives of Civil and Mechanical Engineering, Vol. 18 (2018) No. 3, p. 948-955.
8. Greco S, Gutzeit K, Hotz H, et al. Selective laser melting (SLM) of AISI 316L—impact of laser power, layer thickness, and hatch spacing on roughness, density, and microhardness at constant input energy density. The International Journal of Advanced Manufacturing Technology. Vol. 108 (2020) No. 5, p. 1551-1562.
9. Gao P, Wei K, Yu H, et al. Influence of layer thickness on microstructure and mechanical properties of selective laser melted Ti-5Al-2.5 Sn alloy. Acta Metall Sin. Vol. 54 (2018) No. 7, p. 999-1009.
10. Shi W, Wang P, Liu Y, et al. Properties of 316L formed by a 400 W power laser Selective Laser

Melting with 250 μm layer thickness. Powder Technology. Vol. 360 (2020) p. 151-164.

11. Shi X, Yan C, Feng W, et al. Effect of high layer thickness on surface quality and defect behavior of Ti-6Al-4V fabricated by selective laser melting. Optics & Laser Technology. Vol. 132 (2020) p. 106471.
12. Shi W, Liu Y, Shi X, et al. Beam diameter dependence of performance in thick-layer and high-power selective laser melting of Ti-6Al-4V. Materials. Vol. 11 (2018) No. 7, p. 1237.
13. Simonelli M, Tse Y Y, Tuck C. Effect of the build orientation on the mechanical properties and fracture modes of SLM Ti–6Al–4V. Materials Science and Engineering: A. Vol. 616 (2014) p. 1-11.
14. Vrancken B, Thijs L, Kruth J P, et al. Heat treatment of Ti6Al4V produced by Selective Laser Melting: Microstructure and mechanical properties. Journal of Alloys and Compounds. Vol. 541 (2012) p. 177-185.
15. Wycisk E, Siddique S, Herzog D, et al. Fatigue performance of laser additive manufactured Ti–6Al–4V in very high cycle fatigue regime up to 109 cycles. Frontiers in Materials. Vol. 2 (2015) p. 72.
16. Yu H, Li F, Wang Z, et al. Fatigue performances of selective laser melted Ti-6Al-4V alloy: Influence of surface finishing, hot isostatic pressing and heat treatments. International Journal of Fatigue. Vol. 120 (2019) p. 175-183.